Draft version March 13, 2024
Typeset using LaTeX **twocolumn** style in AASTeX631

Type IV-like Solar Radio Burst Consisting of a Series of Spikes Observed by PSP

Bing Ma(马兵) [1], Ling Chen(陈玲) [1,2], De-Jin Wu(吴德金) [1,2], Marc Pulupa [3] and Stuart D. Bale [3,4,5,6]

[1] *Key Laboratory of Planetary Sciences, Purple Mountain Observatory, Chinese Academy of Sciences, Nanjing 210023, People's Republic of China*
[2] *CAS Center for Excellence in comparative Planetology, Hefei 230026, People's Republic of China*
[3] *Space Sciences Laboratory, University of California, Berkeley, CA 94720-7450, USA*
[4] *Physics Department, University of California, Berkeley, CA 94720-7300, USA*
[5] *The Blackett Laboratory, Imperial College London, London, SW7 2AZ, UK*
[6] *School of Physics and Astronomy, Queen Mary University of London, London E1 4NS, UK*

(Received ?; Revised ?; Accepted ?)

Submitted to ApJL

ABSTRACT

Solar and interplanetary radio bursts can reflect the existence and motion of energetic electrons and are therefore a kind of vital phenomenon in solar activities. The present study reported a solar radio burst (SRB) event observed by Parker Solar Probe (PSP) in its 8th orbital encounter phase, and it lasted about 20 hours in a frequency range of 0.5-15 MHz, called the type IV-like SRB. This type IV-like SRB consists of a series of numerous spikes with the center-frequency drifting slowly from ∼5 MHz to ∼1 MHz, and each individual spike appears a much faster frequency drifting and has a narrow frequency range of a few MHz and short duration of a few minutes. Based on the empirical models of the solar atmosphere adopted commonly, combining the in-situ measurement by PSP, we propose that these small-scale spikes were generated by a group of solitary kinetic Alfvén waves (SKAWs) in a magnetic loop accompanying coronal mass ejection (CME) and moving outwards, in which the frequency drifting of individual spike is caused by the SKAW's propagation and the center-frequency drifting may be attributed to the motion of the magnetic loop.

Keywords: Solar radio emission, Interplanetary physics

1. INTRODUCTION

As the obvious sign of energetic electrons, solar radio bursts (SRBs) are the important phenomenon and indispensable way to investigate solar eruption activities and the correlated electron acceleration processes. Wild & McCready (1950) completed the early observations for SRBs at 70-130 MHz and classified them into three types (type I, II and III) according to their different frequency drift rates. Subsequently, type IV and V radio bursts were found and reported by other researchers (Boischot 1957; Kundu 1961; Weiss 1963; Suzuki & Dulk 1985). Depending on the location of the radiation source, the SRBs could be classified as coronal (25-300 MHz) and interplanetary (IP, 0.01-10 MHz) radio bursts (Lobzin et al. 2014).

The most frequently observed IP radio bursts are type III radio bursts, which can be identified by the fast frequency drift from high to low frequency and are triggered by fast electron beams associated with the violent energy release processes such as solar flare (Reid & Ratcliffe 2014). With much slower frequency drift rate, the type II SRBs are usually associated with coronal mass ejections (CME) and are believed to be excited by the shock-accelerated energetic electrons (Warmuth 2007; Vršnak & Cliver 2008). Type IV radio bursts are a kind of broadband radio continua, which are deemed to be produced by non-thermal electrons confined in closed magnetic structure and plasmoids (Hillaris et al. 2016).

Corresponding author: Ling Chen
clvslc214@pmo.ac.cn

In general, the radio radiation below ∼10 MHz from high corona and interplanetary space cannot be detected by the ground-based radio telescope due to the shielding effect of Earth's ionosphere. Therefore, the radio observation by spacecraft, especially the Parker Solar Probe (PSP) in the near-Sun orbit, is necessary for the investigation of low frequency radio bursts. PSP can measure electric and magnetic field of the near-Sun solar wind (Fox et al. 2016) and support a great opportunity to observe radio bursts generated from high corona and interplanetary space. Ma et al. (2021, 2022) reported that many weak SRBs observed by PSP near its orbital perihelion can hardly be detected by WIND in Sun-Earth L1 point due to the radiation attenuation effect. Recently, Chen et al. (2024) reported that a kind of weak SRBs with narrow frequency range (hundreds of kHz to dozens of MHz) and short duration (a few minutes) observed by PSP when it approached the perihelion of the second orbit and crossed a magnetic channel with low density. These weak SRBs with small-scale emitting sources originated from the typical solar wind acceleration region based on the empirical models of solar atmosphere. The relative frequency drift rates of these events decrease from > 0.01 s^{-1} to < 0.01 s^{-1}, implying that their emission sources experience strong evolution. Chen et al. (2024) proposed that these weak small-scale SRBs are triggered by energetic electrons accelerated by solitary kinetic Alfvén wave (SKAW) with the kinetic scale of plasma particles, called solitary wave radiation (SWR).

In this work, we report an SRB event lasting for about 20 h, which was detected by PSP near the perihelion of its eighth orbit but not by farther spacecraft and ground-based instruments due to its weak intensity and radiation attenuation. It consists of numerous weak radio spikes with the center-frequency drifting slowly from ∼5 MHz to ∼1 MHz, however, each individual spike appears a much faster frequency drifting. Combing the approach observed data by PSP and much farther measurements by other space and ground-based instruments, we analyze the observed characteristics and possible generation mechanism of this SRB event, called the type IV-like SRB. The rest of this letter is arranged as follows: Section 2 introduces the instruments and main features of the event. Section 3 analyzes the possible plasma radial models in the emission source of the event. Finally, Section 4 presents our summary and discussions.

2. INSTRUMENTATION AND OBSERVATION

2.1. *Instrumentation*

Radio dynamic spectrum can provide rich information of energetic electrons and hence is the essential and vital data for the investigation of SRBs. The data from multiple spacecraft including PSP, WIND and Solar TErrestrial RElations Observatory Ahead (STEREO A, Kaiser et al. 2008) are used to checked the radio dynamic spectrum. As a near-Sun spacecraft, PSP flies in elliptical orbits, which perihelion will be closer to the Sun gradually and reach the position where the heliocentric distance R is about $9.86R_\odot$ ($R_\odot$ is the solar radii) in 2024 (Fox et al. 2016). As a section of FIELDS instrument (Bale et al. 2016) on PSP, the radio frequency spectrometer (RFS, Pulupa et al. 2017) can measure the spectrum of radio radiation from 10.5 kHz to 19.2 MHz in a higher time resolution (a spectrum per 7 s in orbit 1-5 and per 3.5 s after orbit 5) at the encounter phases ($R < 0.25$ au).

WIND spacecraft launched in 1995 locates the Sun-Earth L1 point after 2004. STEREO A moves along the heliocentric orbits in a slightly higher speed than the Earth. Both WAVES on WIND spacecraft (Bougeret et al. 1995) and the STEREO/WAVES on STEREO A (Bougeret et al. 2008; Driesman et al. 2008) are the instruments used to measure radio and plasma waves. They can provide the radio observed data with the cadence of a spectrum/min at frequency range 4 kHz - 13.8 MHz (WIND/WAVES) and 2.5 kHz - 16 MHz (STEREO/WAVES), respectively. In addition, Nanay Decameter Array (NDA, Boischot et al. 1980), a ground-based radio telescope is also used to provide the spectrum observation on the higher frequency bands of 15-80 MHz from the perspective of the Earth. The image of white light corona observed by Large Angle Spectroscopic Coronagraph (LASCO, Brueckner et al. 1995) C2 (with the field of view: 1.5-6 $R_\odot$) on the Solar and Heliospheric Observatory (SOHO, locating at Sun-Earth L1 point, Domingo et al. 1995) is used to check the possibly correlative CME.

2.2. *Observation*

Figure 1 shows the radio observation by PSP/RFS from 2021 April 26 10:00 to 27 09:00 and the frequency drift features of eight spikes during this interval. From the radio dynamic spectrum shown in Figure 1(a), an intense type III radio burst was detected from 11:00 to 12:00 on 2021-04-26. After that, a radio burst consisting of numerous weak radio spikes with fast frequency drift appear and last for about 20 hours. The weak spikes exhibit three special spectral features: (1) each of them has a shorter duration of about 1-4 min; (2) the start frequency for most of them is below 15 MHz; (3) their peak frequency decrease with the time. It's worth noting

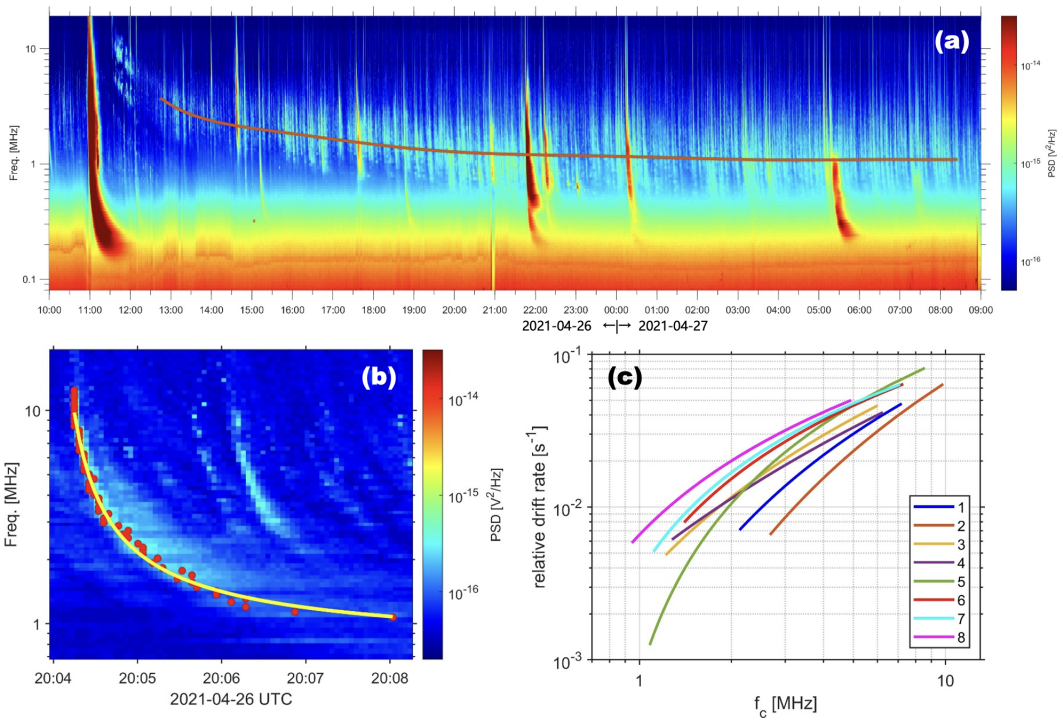

Figure 1. The features of 20-hour radio burst observed by PSP. Panel (a) shows the dynamic spectrum observed by PSP/RFS during the period from 2021-04-26 10:00 to 2021-04-27 09:00. The orange curve shows the trend of slow frequency drift for the center frequencies of spikes. Panel (b) is an example of the method for fitting the drift curve of single spike. The red dots indicate the time of peak intensity at each frequency. The yellow curve is the fitted result of this event. The relative frequency drift rate of eight spikes are shown in panel (c), which is calculated by the fitting data of frequency-time drift using the method in panel (b).

Table 1. The detailed parameters of eight selected weak radio spikes.

No.	start time	duration	$f_{\rm start}$ [MHz]	$f_{\rm end}$ [MHz]	$\rm PSD_{max}$ [lg($\rm V^2$/Hz)]	$\rm flux_{max}$ [$\rm W/m^2$/Hz]
1	2021-04-26 13:06:40	1′51″	8.43	2.13	-15.03	2.25×10^{-18}
2	2021-04-26 14:42:44	1′20″	10.47	2.52	-15.25	1.34×10^{-18}
3	2021-04-26 17:23:10	2′19″	7.08	1.20	-15.33	1.10×10^{-18}
4	2021-04-26 18:41:00	2′12″	6.78	1.27	-14.95	2.64×10^{-18}
5	2021-04-26 20:04:07	4′04″	13.02	1.07	-15.06	2.09×10^{-18}
6	2021-04-27 00:30:35	1′41″	6.48	1.37	-15.00	2.37×10^{-18}
7	2021-04-27 03:04:26	2′16″	7.72	1.07	-15.10	1.89×10^{-18}
8	2021-04-27 06:11:29	2′02″	5.73	0.96	-15.42	8.97×10^{-19}

that this event can hardly be observed by other farther spacecraft and ground-based radio telescope because of its much weak intensity and radiation decay.

The specific type of SRB needs to be determined by their frequency drift rate according to their original definition (Wild & McCready 1950). The absolute frequency drift rate $D_{\rm abs} = |{\rm d}f/{\rm d}t|$ of radio bursts can reflect the motion of radiation source and distinguish the type of radio bursts. However, the difference of $D_{\rm abs}$ in different frequency ranges is relatively large even for the same burst. Therefore, relative frequency drift rate $D_{\rm rel} = |{\rm d}f/(f_c{\rm d}t)|$ is defined to better discriminate the types of bursts at different frequency ranges (Tan et al. 2019), where f_c is the central frequency between the two

frequency point used to calculate $\mathrm{d}f$. For a individual radio burst, the mean relative frequency drift rate can be calculated by the equation $\overline{D}_{\rm rel} = |\Delta f/(f_0 \Delta t)|$, where f_0 is the central frequency of the whole event.

In order to accurately calculate the frequency drift rate of weak radio spikes, we fit the frequency-time drift curve of them. An example of our fitting method is shown in Figure 1(b). By using the noise reduction method introduced in Section 2.2 of Ma et al. (2022), the radio dynamic spectrum unaffected by quasi-thermal noise can be obtained. The frequency drift trend of radio spikes could be obtained by their peak intensity. For the burst displayed in Figure 1(b), we get the red scatter points of peak intensity by finding the time of maximal intensity at each frequency. The yellow curve is the fitting result of red scatter points by using the fitting equation $\lg(f) = at^b + c$, where f and t are frequency and time, and a, b and c are the fitting parameters. It is evident that the fitted curve can well reflect the frequency drift of this event.

Total eight clear and non-overlapping spikes are selected and shown in Table 1 according to the radio dynamic spectrum during the period from 2021 April 26 12:30 to 27 09:00. Figure 1(c) shows their corresponding $D_{\rm rel}$. As the frequency decreases from ∼10 MHz to ∼1 MHz, their $D_{\rm rel}$ values decrease significantly from > 0.01 s^{-1} to < 0.01 s^{-1}. Tan et al. (2019) presented that the $\overline{D}_{\rm rel}$ range of metric-wave type II and III radio bursts are $\leqslant 0.01$ s^{-1} and $\geqslant 0.1$ s^{-1}, respectively. The relative frequency drift rates of these eight spikes are obviously different from the typical type II and III radio bursts, which indicates a series of strong dynamic evolution may happen at emission source, and these spikes may be generated from other small scale electron acceleration process.

As shown in Figure 2(a), a slow and weak CME event was found in the observation of white light coronagraph LASCO/C2 start at about 11:48 on April 26, which is slightly earlier than the onset of these radio spikes. To measure the motion speed of CME, we sliced the image of LASCO/C2 from 10:00 to 18:00 along direction indicated by blue line in Figure 2(a). The time-space diagram obtained by slicing is displayed on Figure 2(b), where the green line marks the leading edge of a distinct bright motive structure in the CME with drift velocity about 149 km/s. This velocity is much lower and possibly cannot be enough to generate shock wave driving type II radio bursts. The Alfvén speed v_A in the emission source is requisite for the further comparison. It will be discussed in detail in Section 3.2.

This CME is the unique eruption event associated with the weak spikes and the former intense type III burst group at almost the same time by checking the multiband observation including Atmospheric Imaging Assembly (AIA, Lemen et al. 2012) aboard Solar Dynamics Observatory (SDO, Pesnell et al. 2012) and the Extreme Ultraviolet Imager (EUI, Rochus et al. 2020) aboard Solar Orbiter (SolO, Forveille & Shore 2020) not shown in this article. According to the positions of spacecraft shown in Figure 2(g), it could be inferred that the associated active region may exist behind the northwestern limb of the Sun (labeled by black arrow). Using the data observed by PSP, NDA, WIND and STEREO A, the multi-view radio observation of the intense type III events on Figure 2(c)-(f) also support this possibility. An intense type III radio burst and its following slow frequency-drift radio emission (such as type II radio burst) possibly originate from the same active region (Pohjolainen & Talebpour Sheshvan 2021). The start time t_1 of this intense type III burst group is different between the observation by PSP near the Sun and the instruments (WIND and NDA) near the Earth because of the enormous difference in their heliocentric distance. The t_1 in PSP's observation is about 10:57:12 while that in NDA and WIND is about 11:07:02. The time delay between them is about $9'\,50''$, which is significantly longer than the light propagation time from the Sun to Earth, i.e., $8'\,18''$. It implies that the type III event generated behind the solar limb so that the PSP on the back of the Sun observed them firstly. Subsequently, the radiation experienced a series of scattering by coronal plasma and partial radiation can propagate towards the Earth direction and then was detected by WIND and NDA. In other words, the scattering process extend the propagation time of the radiation. Therefore, we propose that the intense type III burst group and the subsequent radio event consisting of many spikes are probably excited by flare and the following CME originated from the limb-behind active region.

3. PLASMA MODELS AND THEORETICAL EXPLANATION

3.1. *Selection of plasma radial models*

In order to further investigate the radiation mechanism of this event, reliable empirical models of coronal plasma are indispensable. Leblanc et al. (1998) presented the $n_{e-\rm Lebl}$ model from the corona to 1 au based on the radio observation by WIND spacecraft, which is a widely adopted electron density model due to its reasonability. It can be expressed by the form $n_e = ar^{-2} + br^{-4} + cr^{-6}$, where r is the heliocentric distance in units of $\mathrm{R}_\odot$, and a, b, c are the fitted parameters. The terms proportional to r^{-6} and r^{-2} are dominant at relatively static high corona from $\sim 1.3\mathrm{R}_\odot$ to

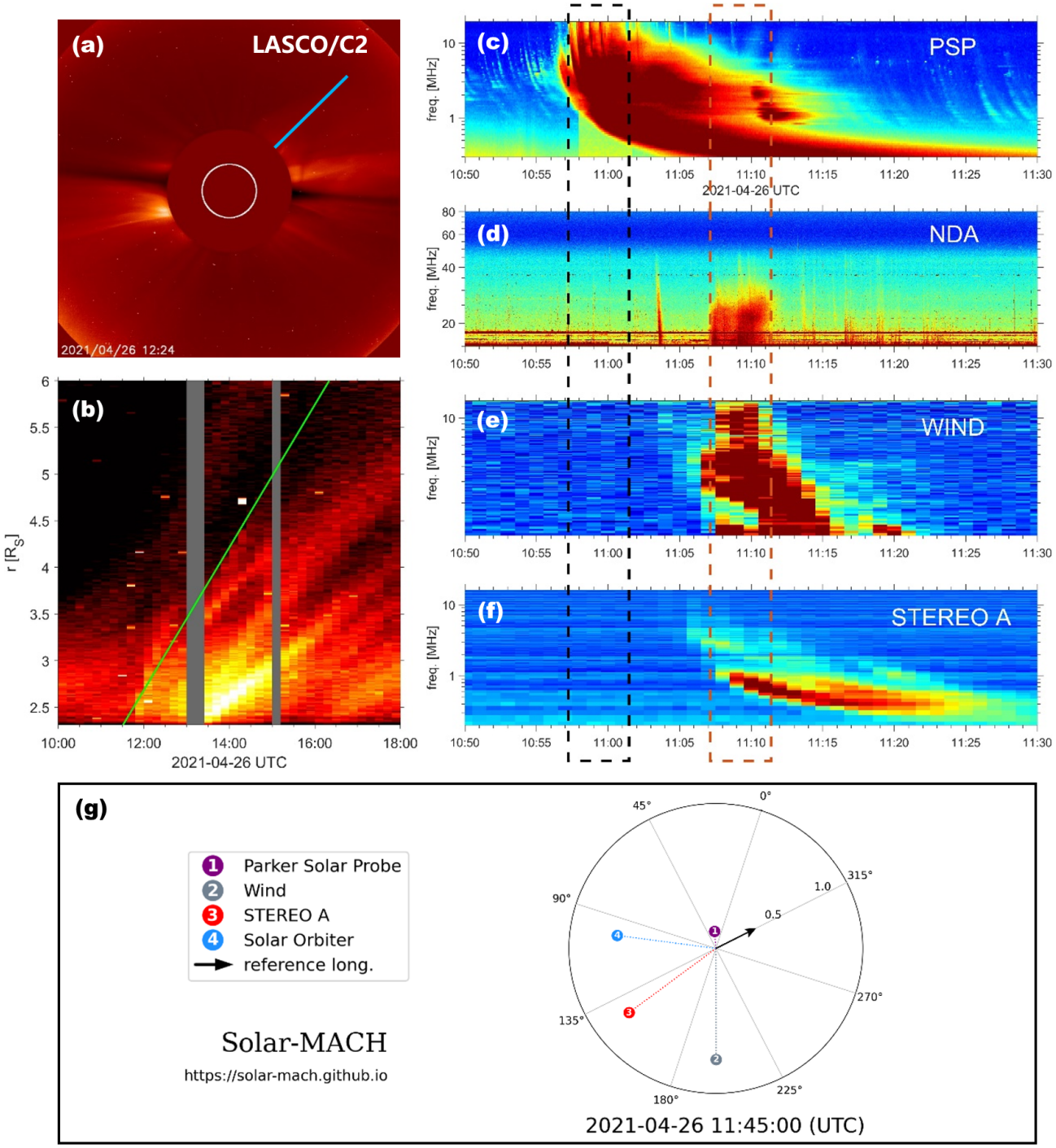

Figure 2. Multiband observation of correlative solar eruption events and the positions of the used spacecraft. White light coronal observation by LASCO/C2 of SOHO is shown in panel (a). The blue line indicates the position of slice used to calculate the motion velocity of bright structure in the CME. Panel (b) is the space-time slice diagram from 10:00 to 18:00 on 2021 April 26 at the blue line in panel (a). The green line in panel (b) indicates the leading edge of a obvious bright structure. Panel (c)-(f) are the radio dynamic spectra observed by PSP/RFS, NDA, WIND/WAVES and S/WAVES on STEREO A. The black dashed box indicates the duration of intense type III burst group at the highest frequency in PSP's dynamic spectrum. And the brown dashed box marks the duration of that obseved by NDA and WIND. Panel (g) shows the position diagram of PSP, WIND, STEREO A and Solar Orbiter, ploted by Solar-MACH program (Gieseler et al. 2023). The black arrow marks the possible ejection direction of CME.

$\sim 3R_\odot$ and the dynamic solar wind in the interplanetary space from dozens of $R_\odot$ to beyond 1 au, respectively. The term proportional to r^{-4} was used to fit the transition from the high corona to the interplanetary space. In order to fit the much higher electron density about 10^{10} cm^{-3} at lower corona, Wu & Fang (2003) added the exponential term $10^{10}e^{-50(r-1)}$ to the model $n_{e-\mathrm{Lebl}}$ of Leblanc et al. (1998).

In addition, Mariani & Neubauer (1990) proposed the magnetic field models in the form of $B(r) = Ar^{-3} + Br^{-2}$, where the items proportional to r^{-3} and r^{-2} can well reflect the dipole magnetic field of the active region and the monopole field in the farther interplanetary space. Using the in situ plasma measurement by PSP, Chen et al. (2021) fitted the models of Mariani & Neubauer (1990) and then presented the model $n_{e-\mathrm{Chen}}$ and B_{Chen} (see the Equation (1) and (2) in Chen et al. 2021). These models also used to explain the high-coronal and interplanetary radio bursts observed by PSP during its second orbital encounter phase.

To precisely match the observed events in present work, we fitted the parameters of $n_{e-\mathrm{Chen}}$ and B_{Chen} based on PSP's in situ detection results (mean proton density $\overline{n}_p = 196.2$ cm^{-3} and mean magnetic field $\overline{B} = 1.3\times10^{-3}$ G) during the period from 09:00 on April 26 to 09:00 on April 27. The obtained model is listed as follows:

$$n_e(r) = \frac{n_0}{1 + 9e^{-(r-1)^2/100}}, \tag{1}$$

$$n_0 = \frac{10^{10}}{e^{50(r-1)}} + 0.71\left(\frac{680}{r^4} + \frac{35}{r^2} + 2.8\right)\frac{10^5}{r^2} \ \left[\mathrm{cm}^{-3}\right], \tag{2}$$

$$B(r) = 15r^{-3} + 0.87r^{-2} \ [\mathrm{G}]. \tag{3}$$

Figure 3 shows the $n_e(r)$ and $B(r)$ models in panels (a) and (b) and their corresponding characteristic frequencies f_{pe} and f_{ce} in panel (c), respectively. For the fundamental-frequency emission, the characteristic frequency reflects the emitting frequency of radio bursts by the corresponding emission mechanism. From the dynamic spectrum shown in Figure 1(a), one can find that the frequency range of these weak radio spikes is approximately 0.5-15 MHz, which is labeled by the thin horizontal dotted lines in Figure 3 (c). It is obvious that the f_{ce} is larger than f_{pe} in the frequency range of radio spikes. It implies these spikes might be explained by the ECM emission mechanism rather than plasma emission.

3.2. *Theoretical Explanation of Weak Radio Spikes and Long-time Emission*

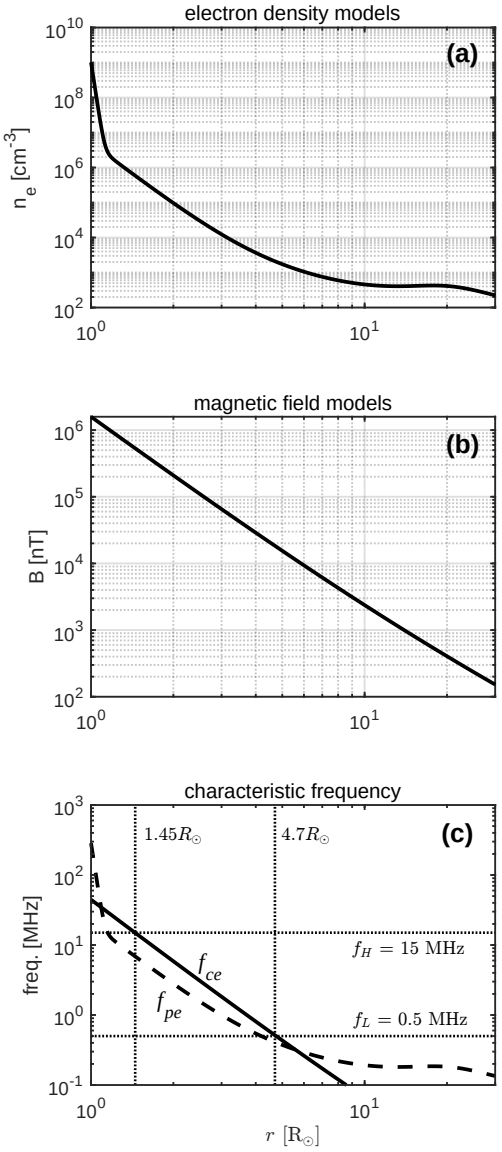

Figure 3. Plasma radial models and their corresponding plasma characteristic frequencies. Panel (a) and (b) show the electron density model $n_e(r)$ and magnetic field model $B(r)$, respectively. The corresponding f_{pe} (thick dashed lines) and f_{ce} (thick solid lines) are shown in panel (c). The thin dotted lines mark the higher and lower frequency limits of the observed radio spikes (f_H and f_L) and their corresponding heliocentric distances ($1.45R_\odot$ and $4.7R_\odot$).

The analysis of observed dynamic spectrum in Figure 1(a) shows that most of weak spikes have low start frequency ($\leqslant$ 15 MHz), narrow frequency range (a few MHz), short duration (1-4 min) and weak peak intensity ($\sim 10^{-15}$ V^2/Hz). Furthermore, the weak spikes also have much higher occurrence rate (on average $\sim$ 1 event/min). These characteristics imply that the weak spikes may originate from small-scale emitting sources at high corona rather than the energetic electron beams

accelerated in low corona. All the features of the spikes mentioned above are consistent with the solitary wave radiation (SWR) presented by Chen et al. (2024).

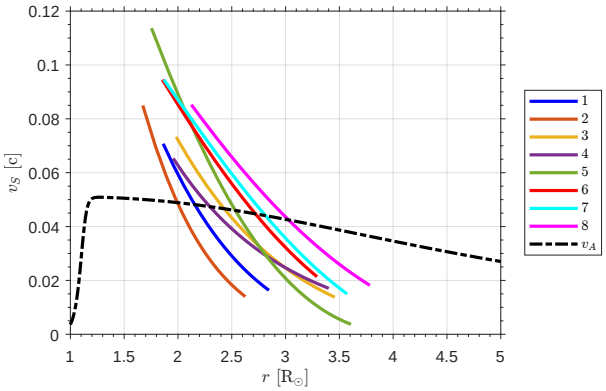

Figure 4. Drift speed v_S of emission source of the selected eight spikes on the assumptions of ECM emission. The colorful solid curves and the black dashed curve indicate v_S of eight events and the Alfvén speed v_A, respectively. The v_S is calculated by the models of magnetic field and electron density at present work.

Based on the plasma parameter models presented in Section 3.1, the condition $f_{ce} > f_{pe}$ shown in Figure 3(c) means that the ECM instability can be responsible for the generation of the radio emission of these weak spikes. Combining the magnetic field model (Equation (3)) and the absolute frequency drift rate $D_{\rm abs}$ of the eight spikes shown in Figure 1(c), we calculate the motion speed v_S of their emitting sources by using the following equation:

$$D_{\rm abs} = \frac{{\rm d}f_{ce}}{{\rm d}t} = \frac{{\rm d}f_{ce}}{{\rm d}r}\frac{{\rm d}r}{{\rm d}t} = \frac{{\rm d}f_{ce}}{{\rm d}r}v_S. \quad (4)$$

The colorful curves in Figure 4 show the v_S for the eight events in units of light speed c versus the heliocentric distance of emitting source. The black dashed curve shows the Alfvén speed v_A of the ambient plasma. One can find that the v_S decrease from $\sim 0.1c$ ($> v_A$) to $\sim 0.02c$ ($< v_A$), which implies that these weak spikes are possibly not common type III SRBs excited by fast electron beams, and they should be excited by energetic electrons accelerated by small-scale plasma waves. Therefore, we suggest that the spikes can be explained using the SWR theoretical model proposed by Chen et al. (2024).

Kasper et al. (2021) found that strong Alfvén turbulence is ubiquitous in the coronal plasma with sub-Alfvénic stream. The Alfvén wave can extend to the kinetic scale and become kinetic Alfvén wave (KAW, Wu & Chen 2020) by the anisotropic turbulent cascade (Goldreich & Sridhar 1995; Tsurutani et al. 2018). Simultaneously, the nonlinear solitary wavelets of KAW (SKAW) can form easily in the low β plasma, because Landau damping is too weak to dissipate the KAW effectively when its phase speed ($> v_A$) is significantly larger than the electron thermal speed (v_{Te}). The electrons can be trapped and accelerated effectively to the velocity much higher than the propagating speed of SKAW and excite radio emission via ECM instability (Chen et al. 2024).

For the generation process of radio emission, the AWs also have significant impact on the ECM instability (Wu et al. 2012; Wu 2014; Zhao et al. 2015; Chen et al. 2017, 2021). The excitation of ECM instability need the free energy in the direction perpendicular to the magnetic field, i.e., $\partial F(v)/\partial v_\perp > 0$, where the $F(v)$ is the velocity distribution function (VDF) of electrons. AWs can scatter the energetic electrons to the so-called crescent-shaped distribution, which can provide transverse free energy to excite ECM emission effectively. Chen et al. (2024) calculated the growth rate of possible wave modes using the crescent-shaped VDF, and the result shows that the fundamental wave of O-mode have much higher growth rate than the harmonic wave of O-mode and X-mode. We have checked the Stokes V/I parameter of these radio spikes using the method from Pulupa et al. (2020). The result shows that their average degree of polarization is about 0.3, which means these spikes have partial left-hand circular (LHC) polarization (O-mode emission). It is different from the fully O-mode emission excited by ECM instability probably owing to the propagation effect or the simultaneous O-mode and X-mode emission.

The propagation of SKAW carrying the energetic electrons causes the frequency drift of the weak spikes. Therefore, the decay of v_S demonstrate that the SKAW will decelerate as propagating by possible dissipation such as ion-acoustic turbulence and the Coulomb collision (Wahlund et al. 1994; Voitenko & Goossens 2000; Wu et al. 2007). The inverse of SKAW damping rate can be the reference of its dissipation time. Using this estimation method, Chen et al. (2024) presented that the dissipation time of SKAW will be shorter than 10 min in the low β plasma of $v_A > v_{Te}$, which correspond with the duration (1-4 min) of the weak radio spikes observed by PSP in this work. Therefore, we suggest that these weak radio spikes are the ECM emission excited by the electrons trapped and accelerated by the electric field of SKAW, i.e., SWR.

The orange curve in Figure 1(a) labels the drift trend of the center frequency of these small-scale spikes, which reflects the motion of the magnetic loop. Using the magnetic field model $B(r)$, we estimated that the moving speed of the magnetic loop V_L decreases from $\sim$120 km/s to $\sim$5 km/s. At the beginning phase, the V_L is slightly

lower than the speed of the CME ($v_{\rm CME} \sim 149$ km/s) shown in Figure 2(a), which implies the radio radiation is associated with the CME. The slow drift of the spike center frequencies reflects the slow motion outwards of the magnetic loop accompanying the CME at the velocity V_L, in which the emitting sources of the small-scale SWRs (i.e., SKAWs) propagate at the velocity V_S along the magnetic field of the loop. Therefore, we suggest that the observed SRB event is a type IV-like SRB that consists of a series of SWRs confined within the magnetic loop moving outwards.

4. SUMMARY AND DISCUSSION

We report a radio burst consisting of a series of weak spikes observed by PSP during the period from 12:30 in 2021 April 26 to 09:00 2021 April 27. The weak radio spikes have several distinct features: lower upper-limit of frequency (< 15 MHz), narrow frequency band (0.5-15 MHz), short duration (< 5 min) and lower peak intensity ($\sim 10^{-15}$ V^2/Hz). The coronagraph observation by SOHO/LASCO shows a temporal-relative weak CME event with the propagation speed about 149 km/s. The simultaneous radio observation by PSP, NDA, WIND and STEREO A shows that the observed time of earlier intense type III radio burst group is obviously different, especially the time delay between NDA (and WIND) near the Earth and PSP is larger than the propagation time of light from the Sun to Earth, which means that the emitting source may locate behind the solar northwestern limb and the radiation experience the scattering by coronal plasma and hence their propagation time may be extended.

The motion of emission sources can be reflected by their $D_{\rm rel}$. The $D_{\rm rel}$ of weak spikes decrease from > 0.01 s^{-1} to < 0.01 s^{-1} implies they are probably not triggered by fast electron beams. To further explore the emission mechanism of the observed radio spikes, we selected appropriate plasma models, i.e., the Equation (1-3). The characteristic frequency relation $f_{ce} > f_{pe}$ indicates that the weak spikes should be ECM emission rather than plasma emission.

We calculate the drift speed of emission sources for the chosen eight weak spikes and the long-time radiation, respectively. The former decrease from super-Alfvénic $\sim 0.1c$ to sub-Alfvénic $\sim 0.02c$, and the latter is slightly lower than the velocity of the correlative CME at the beginning period. Based on the observations and SKAW theory by Chen et al. (2024), we propose a new model as follows to explain the long-time radio burst including many weak spikes. In a close magnetic structure located within a weak CME erupting behind the solar north-western limb, intense Alfvén turbulence in the low β plasma can extend to smaller kinetic scale (KAWs) and form the non-linear SKAW further. The electrons can be trapped in the potential well of SKAW and accelerated to super-Alfvénic speed by the electric field $E_{\parallel}$ of SKAW. The electrons with crescent-shaped VDF scattered by AWs provide transverse free energy and excite ECM emission (i.e. SWR). The numerous SWRs present a long-time radio burst, which can reflect the movement of whole close magnetic structure behind the CME leading edge, called type IV-like radio burst.

In the lack of the in situ measurement at emission source, the theoretical explanation in this work is mainly based on the plasma empirical models. With the maximum year of solar cycle 25 coming and PSP further approaching the Sun, the possibility for the local detection at the emitting source becoming bigger and bigger, and the demonstration of theoretical assumption will be realizable.

The authors thank Jin-Song Zhao, Zong-Jun Ning, Lei Lu, Fu Yu in PMO and Wei Su in SYSU for their valuable discussions and suggestions. The present research at PMO was supported by the Strategic Priority Research Program of the Chinese Academy of Sciences, Grant No. XDB0560000 and NSFC under grant No. 42174195. The authors thank the PSP/FIELDS, WIND/WAVES, NDA and STEREO projects and teams for their instrument maintenance and open data access. The FIELDS experiment on the Parker Solar Probe spacecraft was designed and developed under NASA contract NNN06AA01C. The FIELDS data could be obtained on the website: https://spdf.gsfc.nasa.gov/pub/data/psp/fields/.

REFERENCES

Bale, S. D., Goetz, K., Harvey, P. R., et al. 2016, Space Science Reviews, 204, 49, doi: 10.1007/s11214-016-0244-5

Boischot, A. 1957, Academie des Sciences Paris Comptes Rendus, 244, 1326. https://ui.adsabs.harvard.edu/abs/1957CRAS..244.1326B

Boischot, A., Rosolen, C., Aubier, M., et al. 1980, Icarus, 43, 399, doi: 10.1016/0019-1035(80)90185-2

Bougeret, J. L., Kaiser, M. L., Kellogg, P. J., et al. 1995, Space Science Reviews, 71, 231, doi: 10/bfmj3z

Bougeret, J. L., Goetz, K., Kaiser, M. L., et al. 2008, Space Science Reviews, 136, 487, doi: 10/bjhrcz

Brueckner, G. E., Howard, R. A., Koomen, M. J., et al. 1995, Solar Physics, 162, 357, doi: 10.1007/BF00733434

Chen, L., Ma, B., Wu, D., et al. 2021, The Astrophysical Journal Letters, 915, L22, doi: 10/gk44zk

Chen, L., Wu, D. J., Zhao, G. Q., & Tang, J. F. 2017, Journal of Geophysical Research: Space Physics, 122, 35, doi: 10.1002/2016JA023312

Chen, L., Ma, B., Wu, D., et al. 2024, The Astrophysical Journal, 961, 136, doi: 10.3847/1538-4357/ad0e65

Domingo, V., Fleck, B., & Poland, A. I. 1995, Space Science Reviews, 72, 81, doi: 10.1007/BF00768758

Driesman, A., Hynes, S., & Cancro, G. 2008, Space Science Reviews, 136, 17, doi: 10/fsjzzg

Forveille, T., & Shore, S. 2020, Astronomy & Astrophysics, 642, E1, doi: 10/gjqrkj

Fox, N. J., Velli, M. C., Bale, S. D., et al. 2016, Space Science Reviews, 204, 7, doi: 10.1007/s11214-015-0211-6

Gieseler, J., Dresing, N., Palmroos, C., et al. 2023, Frontiers in Astronomy and Space Sciences, 9, 1058810, doi: 10.3389/fspas.2022.1058810

Goldreich, P., & Sridhar, S. 1995, The Astrophysical Journal, 438, 763, doi: 10.1086/175121

Hillaris, A., Bouratzis, C., & Nindos, A. 2016, Solar Physics, 291, 2049, doi: 10.1007/s11207-016-0946-6

Kaiser, M. L., Kucera, T. A., Davila, J. M., et al. 2008, Space Science Reviews, 136, 5, doi: 10/fhg2kn

Kasper, J. C., Klein, K. G., Lichko, E., et al. 2021, Physical Review Letters, 127, 255101, doi: 10.1103/PhysRevLett.127.255101

Kundu, M. R. 1961, The Astrophysical Journal, 134, 96, doi: 10.1086/147132

Leblanc, Y., Dulk, G. A., & Bougeret, J.-L. 1998, Solar Physics, 183, 165, doi: 10.1023/A:1005049730506

Lemen, J. R., Title, A. M., Akin, D. J., et al. 2012, Solar Physics, 275, 17, doi: 10.1007/s11207-011-9776-8

Lobzin, V. V., Cairns, I. H., & Zaslavsky, A. 2014, Journal of Geophysical Research: Space Physics, 119, 742, doi: 10/f52wfj

Ma, B., Chen, L., Wu, D., & Bale, S. D. 2021, The Astrophysical Journal Letters, 913, L1, doi: 10/gj35wc

Ma, B., Chen, L., Wu, D., Pulupa, M., & Bale, S. D. 2022, The Astrophysical Journal Letters, 932, L26, doi: 10.3847/2041-8213/ac7525

Mariani, F., & Neubauer, F. M. 1990, in Physics of the Inner Heliosphere I: Large-Scale Phenomena, ed. R. Schwenn & E. Marsch, Physics and Chemistry in Space, Space and Solar Phycics (Berlin, Heidelberg: Springer), 183–206, doi: 10.1007/978-3-642-75361-9_4

Pesnell, W. D., Thompson, B. J., & Chamberlin, P. C. 2012, Solar Physics, 275, 3, doi: 10.1007/s11207-011-9841-3

Pohjolainen, S., & Talebpour Sheshvan, N. 2021, Solar Physics, 296, 81, doi: 10/gppxqg

Pulupa, M., Bale, S. D., Bonnell, J. W., et al. 2017, Journal of Geophysical Research: Space Physics, 122, 2836, doi: 10.1002/2016JA023345

Pulupa, M., Bale, S. D., Badman, S. T., et al. 2020, The Astrophysical Journal Supplement Series, 246, 49, doi: 10/gg9694

Reid, H. A. S., & Ratcliffe, H. 2014, Research in Astronomy and Astrophysics, 14, 773, doi: 10/ghcwz7

Rochus, P., Auchère, F., Berghmans, D., et al. 2020, Astronomy & Astrophysics, 642, A8, doi: 10/gjqrkb

Suzuki, S., & Dulk, G. A. 1985, Bursts of Type III and Type V., 289–332. https://ui.adsabs.harvard.edu/abs/1985srph.book..289S

Tan, B., Chen, N., Yang, Y.-H., et al. 2019, The Astrophysical Journal, 885, 90, doi: 10.3847/1538-4357/ab4718

Tsurutani, B. T., Lakhina, G. S., Sen, A., et al. 2018, Journal of Geophysical Research: Space Physics, 123, 2458, doi: 10.1002/2017JA024203

Voitenko, Y., & Goossens, M. 2000, Astronomy and Astrophysics, 357, 1073. https://ui.adsabs.harvard.edu/abs/2000A&A...357.1073V/abstract

Vršnak, B., & Cliver, E. W. 2008, Solar Physics, 253, 215, doi: 10.1007/s11207-008-9241-5

Wahlund, J.-E., Louarn, P., Chust, T., et al. 1994, Geophysical Research Letters, 21, 1831, doi: 10.1029/94GL01289

Warmuth, A. 2007, in The High Energy Solar Corona: Waves, Eruptions, Particles, ed. K.-L. Klein & A. L. MacKinnon, Lecture Notes in Physics (Berlin, Heidelberg: Springer), 107–138, doi: 10.1007/978-3-540-71570-2_6

Weiss, A. A. 1963, Australian Journal of Physics, 16, 526, doi: 10.1071/PH630526

Wild, J. P., & McCready, L. L. 1950, Australian Journal of Scientific Research A Physical Sciences, 3, 387, doi: 10.1071/CH9500387

Wu, C. S., Wang, C. B., Wu, D. J., & Lee, K. H. 2012, Physics of Plasmas, 19, 082902, doi: 10.1063/1.4742989

Wu, D. J. 2014, Physics of Plasmas, 21, 064506, doi: 10.1063/1.4886124

Wu, D.-J., & Chen, L. 2020, Kinetic Alfvén Waves in Laboratory, Space, and Astrophysical Plasmas, Atmosphere, Earth, Ocean & Space (Singapore: Springer Singapore), doi: 10.1007/978-981-13-7989-5

Wu, D. J., & Fang, C. 2003, The Astrophysical Journal, 596, 656, doi: 10.1086/377599

Wu, D. J., Huang, J., Tang, J. F., & Yan, Y. H. 2007, The Astrophysical Journal, 665, L171, doi: 10.1086/521360

Zhao, G. Q., Feng, H. Q., & Wu, D. J. 2015, Physics of Plasmas, 22, 102105, doi: 10.1063/1.4932325